Supplementary Information

Role of Mo and N Doping Ratios in Regulating the Zinc Storage Performance of δ-MnO_2: A Systematic Study from Single to Co-doping

Shaoyan Huang [a], *Shuling Liu* [a, *], *Sha Fan* [b, c], *Rui Su* [a], *Libo Liu* [a], *Deliang Tian* [b, c], *Jinbao Li* [b, c, *], *Jianbo Tong* [a, *]

[a] Department of Chemistry and Chemical Engineering, Shaanxi Collaborative Innovation Center of Industrial Auxiliary Chemistry & Technology, Key Laboratory of Auxiliary Chemistry and Technology for Chemical Industry, Ministry of Education, The Youth Innovation Team of Shaanxi Universities, Shaanxi University of Science and Technology, Xi'an, Shaanxi, 710021, China

[b] College of Bioresources Chemical & Materials Engineering, Shaanxi University of Science & Technology, Xi'an, Shaanxi, 710021, China

[c] National Demonstration Center for Experimental Light Chemistry Engineering Education, Shaanxi Provincial Key Laboratory of Papermaking Technology and Specialty Paper Development, Xi'an, Shaanxi, 710021, China

[*]Corresponding author.

E-mail address: shulingliu@aliyun.com (Shuling Liu); lijinbao@sust.edu.cn (Jinbao Li); jianbotong@aliyun.com (Jianbo Tong)

Section 1 Experimental Methods

1.1. Preparation of cathode materials

The as-prepared active material was thoroughly mixed with carbon black and polyvinylidene fluoride (PVDF) in a weight ratio of 7:2:1 using N-Methyl-2-pyrrolidone (NMP) solvent to obtain a homogeneous slurry. Subsequently, the slurry was evenly coated onto titanium foil and dried overnight at 80 ℃ under vacuum conditions. The dried electrodes were then punched into circular discs with a diameter of 12 mm, achieving an active material loading of approximately 0.6 mg cm^{-2}.

1.2. Assembly of button batteries

The button batteries were assembled the air using CR2032 types, of which zinc metal as anodes, Whatman GF/A glass fiber filter paper as separators, and material prepared was the positive electrode. Meanwhile, the electrolyte was composed of a mixture of 2 M $ZnSO_4$ and 0.1 M $MnSO_4$.

1.3. Electrochemical performance test

The Cyclic voltammetry (CV) curves were obtained by electrochemical workstation (CHI760E, Shanghai Chenhua Technology Co., LTD., China) at the specified scan rate within a voltage of 0.9 V ~ 1.9 V. The Electrochemical impedance spectroscopy (EIS) tests were implemented on CHI760E within a frequency of 0.01 Hz ~ 100 kHz. Besides, the cycling performance, rate capabilities, galvanostatic Intermittent Titration Technique (GITT), and galvanostatic (dis-)charge profiles were measured between 0.9 V ~ 1.9 V by the CT-4008Tn (Neware/Neware BTS, Shenzhen NEWARE Technology Co., LTD., China).

1.4. Material structure characterization

The morphology and structure of the samples were observed by field emission scanning electron microscopy (SEM), and the element distribution was analyzed by energy dispersion spectrometer (EDS) (SU 8100, Hitachi, Japan). The morphology of the samples was observed by field emission transmission electron microscope (TEM) (JEM-2100-F, JEOL, Japan). Material bonding was determined using X-ray photoelectron spectroscopy (XPS) (K-Alpha, Kratos, UK). X-ray diffraction (XRD) (D8 Advance, Bruker, Germany) was used to analyze the crystalline structure of the products. The Raman spectra were collected on the Raman spectrometer (DXRxi, THEM, USA).

Section 2 Supporting image

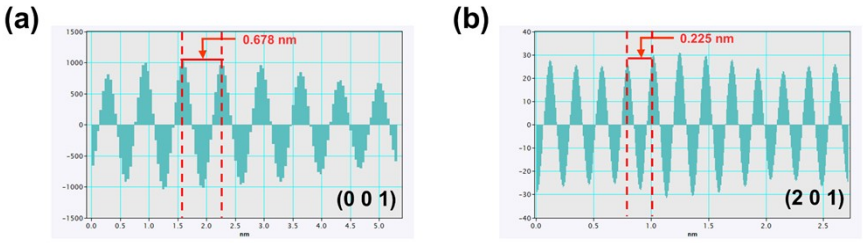

Fig. S1. Lattice parameter measurement and calculation methods.

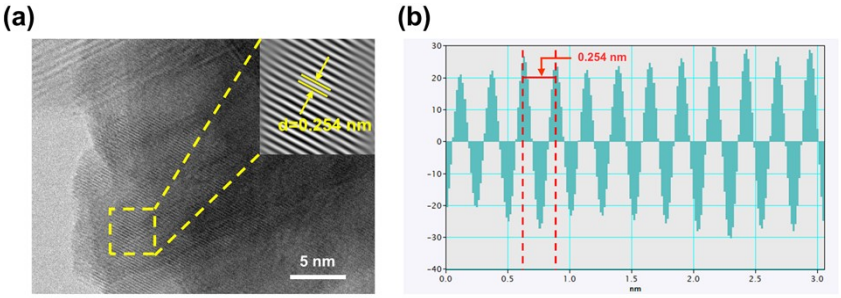

Fig. S2. a) Lattice parameters and b) measured results of δ-MnO_2.

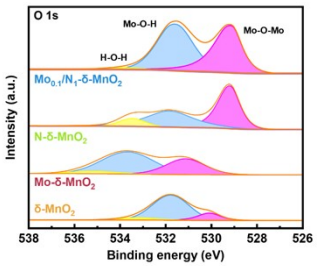

Fig. S3. O 1s XPS spectra of different materials.

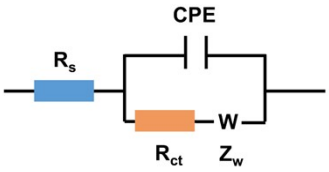

Fig. S4. Schematic representation of the equivalent circuit diagram utilized in EIS.

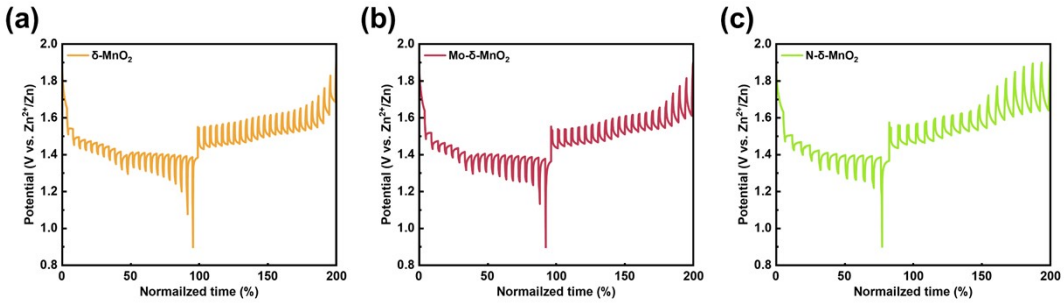

Fig. S5. GITT tests of different cathodes.

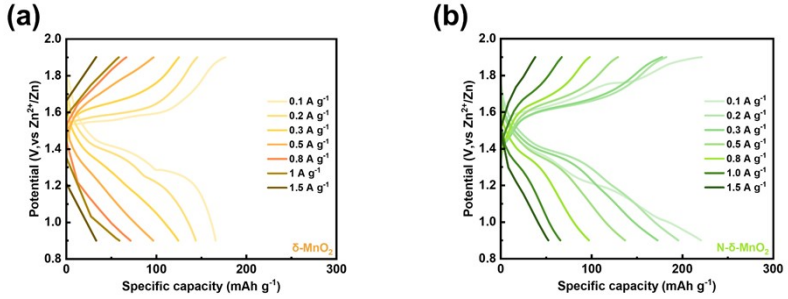

Fig. S6. Charge-discharge curves of a) δ-MnO_2; b) N-δ-MnO_2 under rate capability tests.

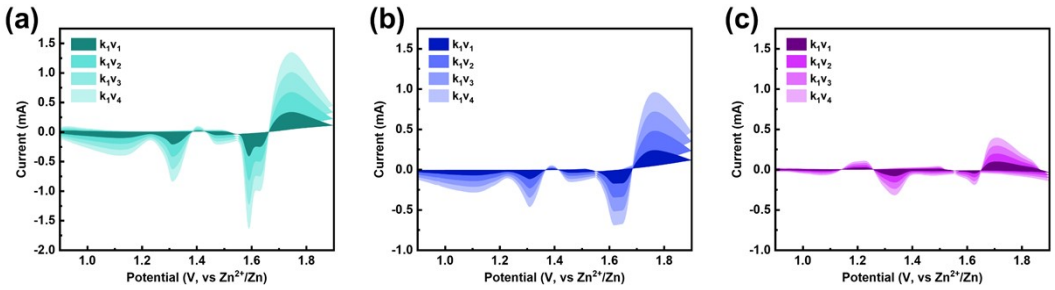

Fig. S7. Impedance capacitance contribution ratio chart of a) $Mo_{0.1}/N_1$-δ-MnO_2 b) $Mo_{0.1}/N_2$-δ-MnO_2 and c) $Mo_{0.2}/N_1$-δ-MnO_2.

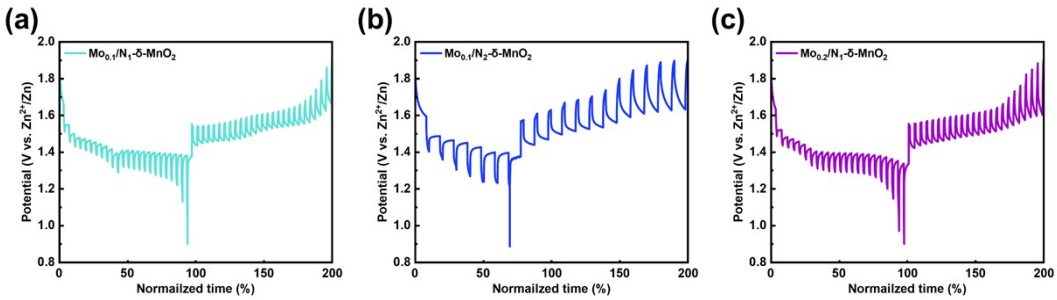

Fig. S8. GITT curves of a) $Mo_{0.1}/N_1$-δ-MnO_2 b) $Mo_{0.1}/N_2$-δ-MnO_2 and c) $Mo_{0.2}/N_1$-δ-MnO_2.

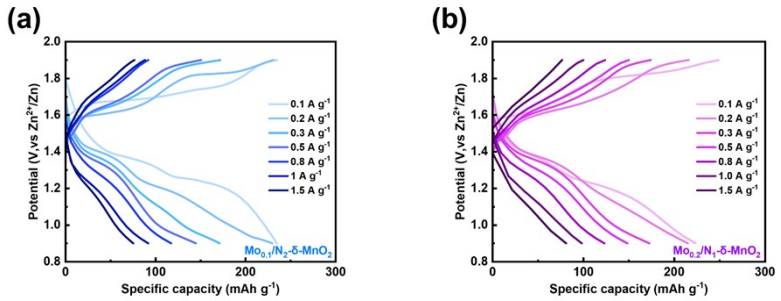

Fig. S9. Charge-discharge curves of a) $Mo_{0.1}/N_2$-δ-MnO_2; b) $Mo_{0.2}/N_1$-δ-MnO_2 under rate capability tests.

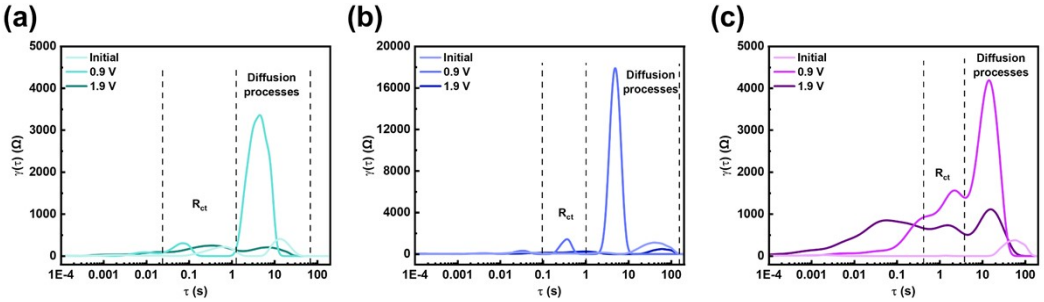

Fig. S10. The DRT curves of different batteries: a) $Mo_{0.1}/N_1$-δ-MnO_2; b) $Mo_{0.1}/N_2$-δ-MnO_2; c) $Mo_{0.2}/N_1$-δ-MnO_2.

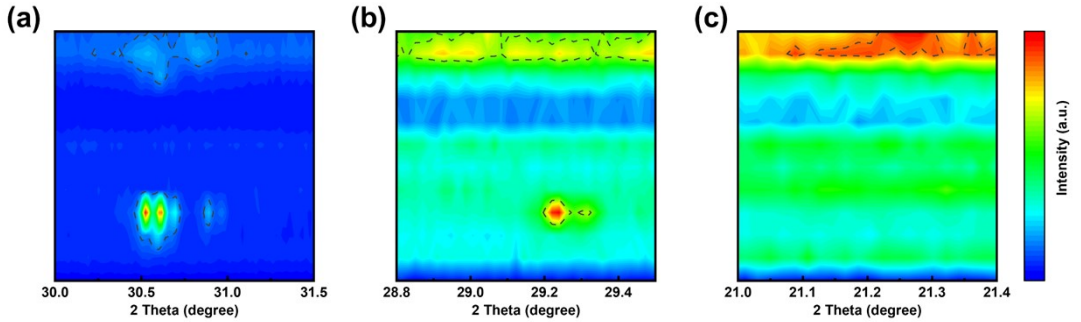

Fig. S11. Corresponding high-resolution Ex-situ XRD patterns.

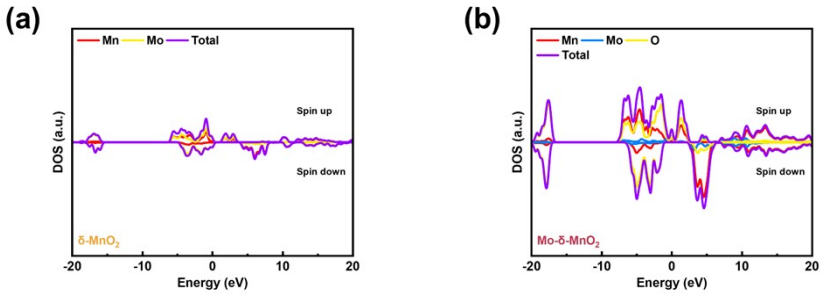

Fig. S12. The calculated density of states (DOS) for a) δ-MnO_2 and b) Mo-δ-MnO_2.

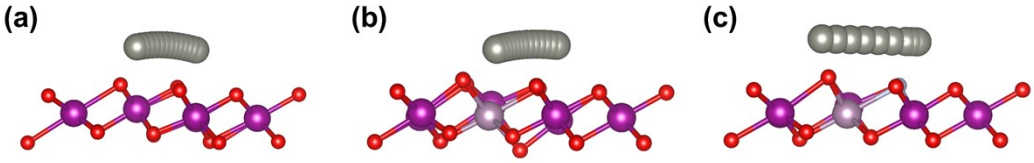

Fig. S13. Zn^{2+} migration pathways of a) δ-MnO_2, b) Mo-δ-MnO_2 and c) Mo/N-δ-MnO_2.

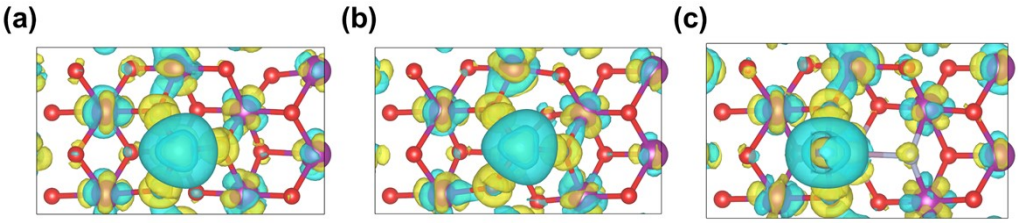

Fig. S14. Charge difference density of a) δ-MnO_2, b) Mo-δ-MnO_2 and c) Mo/N-δ-MnO_2.

Table S1. Comparison with other works.

references	current density (A g^{-1})	Cycle number	Initial discharge specific capacity (mAh g^{-1})	Remaining discharge specific capacity (mAh g^{-1})
1	0.5	300	173.06	113.87
2	0.5	100	351.7	327.3
3	0.1	100	370.38	161.34

4	0.2	150	409	271
5	0.1	70	491.7	250
6	1	300	260	190
This work	0.2	200	370.8	270.0

1 J. Hua, X. Wu, F. Xie, M. Wu, Cr-doping δ-MnO_2 as the cathode material for aqueous zinc-ion batteries, *Surf. Interfaces* 2025, **62**, 106312. https://doi.org/10.1016/j.surfin.2025.106312.

2 Y. Zhao, Y. Zhang, X. Ma, A. Su, Z. Chen, X. Zhang, Vanadium dopant induced the small and low crystallinity layered MnO_2 supported on the carbon nanosheets for high-performance aqueous zinc-ion batteries, *J. Colloid Interface Sci.* 2026, **703**, 139152. https://doi.org/10.1016/j.jcis.2025.139152.

3 T. Zhang, J. Wu, Y. Wang, L. Zhang, F. Ran, Regulating surface bonding network and inner crystal structure to boost Zn storage capacity of flexible MnO_2 cathode, *Chem. Eng. J.* 2025, **511**, 161927. https://doi.org/10.1016/j.cej.2025.161927.

4 R. Han, Y. Pan, C. Du, Y. Xiang, Y. Wang, H. Zhu, C. Yin, Eu doping β-MnO_2 as cathode materials for high specific capacity aqueous zinc ion batteries, *J. Energy Storage* 2024, **80**, 110250. https://doi.org/10.1016/j.est.2023.110250.

5 B. Hu, H. Li, M. Wang, Z. Rao, L. Hao, X. Yu, M. Zhang, Ag-modulated mesoporous δ-MnO_2 cathodes mitigate pseudo-capacitance and enhance specific capacity of aqueous zinc ion batteries, *J. Energy Storage* 2026, **141**, 118975. https://doi.org/10.1016/j.est.2025.118975.

6 J. Yang, Z. Yu, F. Zhang, J. Zheng, J. Zhao, X. Wang, K^+ doped δ-MnO_2 hollow microspheres assembled from ultrathin nanosheets with controlled shell structures for aqueous zinc-ion batteries, *J. Energy Storage* 2026, **143**, 119748. https://doi.org/10.1016/j.est.2025.119748.